MFN= 006229
01 SID/SCD
02 5993
03 INPE-5993-PRE/2108
04 MET
05 S
06 as
10 Mahfouf,J.-F.
10 Manzi, Antonio Ocimar
10 Noilhan, J.
10 Giordani, H.
10 Deque, M.
12 The land surface scheme ISBA within the meteo-france climate model ARPEGE. Part I: implementation and preliminary results
14 2039-2057
30 Journal of Climate
31 8
32 8
40 En
41 En
42 <E>
58 DCM
61 <PI>
64 Aug. <1995>
68 PRE
76 CIENCIAS METEOROLOGICAS
82 <AMAZONIA (REGIAO)>
83 This paper describes recent developments in climate modeling at Meteo-France related to land surface processes. The implementation of a simple land surface parameterization, Interactions between Soil Biosphere Atmosphere (ISBA), has gained from previous validations and calibrations at local scale against field datasets and from aggregation procedures devised to define effective land surface properties. Specific improvements for climate purposes are introduced: spatial variability of convenctive rainfall in canopy drainage estimation and subsurface gravitational percolation. The methodology used to derive climatological maps of land surface parameters at the grid-scale resolution of the model from existing databases for soil and vegetation types at global scale is described. A 3-yr integration for the present day climate with a T42L30 version of the climate model has been performed. Results obtained compare favorably with available observed climatologies related to the various components of the continental surface energy and water budgets. Differences are due mostly to a poor simulation of the precipitation field. However, some differences suggest specific improvements in the surface scheme concerning representation of the bare soil albedo, the surface runoff, and the soil moistured initialization. As a first step prior to tropical deforestation experiments presented in Part II, regional analyses over the Amazon forest indicate that the modeled evaporation and net radiation are in good agreement with data collected during the Amazon Region Micrometeorological Experiment campaign .
87 MICROMETEOROLOGIA
87 ISBA
87 MODELOS
87 ARPEGE
87 INTERACAO

The Land Surface Scheme ISBA within the Météo-France Climate Model ARPEGE. Part I: Implementation and Preliminary Results

J.-F. MAHFOUF*

Météo-France/CNRM, Toulouse, France

A. O. MANZI

Instituto Nacional De Pesquisas Espaciais, São José Dos Campos, Brasil

J. NOILHAN, H. GIORDANI, AND M. DÉQUÉ

Météo-France/CNRM, Toulouse, France

(Manuscript received 14 July 1994, in final form 28 February 1995)

ABSTRACT

This paper describes recent developments in climate modeling at Météo-France related to land surface processes. The implementation of a simple land surface parameterization, Interactions between Soil Biosphere Atmosphere (ISBA), has gained from previous validations and calibrations at local scale against field datasets and from aggregation procedures devised to define effective land surface properties. Specific improvements for climate purposes are introduced: spatial variability of convective rainfall in canopy drainage estimation and subsurface gravitational percolation. The methodology used to derive climatological maps of land surface parameters at the grid-scale resolution of the model from existing databases for soil and vegetation types at global scale is described. A 3-yr integration for the present day climate with a T42L30 version of the climate model has been performed. Results obtained compare favorably with available observed climatologies related to the various components of the continental surface energy and water budgets. Differences are due mostly to a poor simulation of the precipitation field. However, some differences suggest specific improvements in the surface scheme concerning representation of the bare soil albedo, the surface runoff, and the soil moisture initialization. As a first step prior to tropical deforestation experiments presented in Part II, regional analyses over the Amazon forest indicate that the modeled evaporation and net radiation are in good agreement with data collected during the Amazon Region Micrometeorological Experiment campaign.

Introduction

Many sensitivity experiments have shown the importance of land surface processes on the atmospheric general circulation. (e.g., Charney et al. 1977; Shukla and Mintz 1982; Sud et al. 1988). The sensitivity is dominant over tropical regions where the circulation is driven by deep moist convection supplied by surface evaporation and low-level moisture convergence.

Important progress has been achieved in this area during the last 10 years. Realistic surface schemes representing heat and water transfers between soil, vegetation, and the atmosphere have been developed for climate models. The initiative of Dickinson (1984) with the Biosphere Atmosphere Transfer Scheme (BATS) and Sellers et al. (1986) with the Simple Biosphere Model (SiB) were followed by many others who have taken part in the recent intercomparison project PILPS (Henderson-Sellers et al. 1993). Databases describing soil and vegetation types at global scale were constructed for use in general circulation models (GCMs) (Matthews 1985; Wilson and Henderson-Sellers 1985). Finally, pilot experiments have started that are devoted to documenting the various components of the water and energy balance (surface, atmosphere, subsurface) on the grid scale of GCMs. The objective is to evaluate, calibrate, and improve land surface parameterization schemes for numerical models. The need to investigate areas larger than the local scale meant the development of aggregation procedures that could take into account subgrid-scale variability and define properties or processes at the scale resolved by GCMs. Two main tools are used to achieve this goal: mesoscale models and remote sensing techniques. The first experiment of this kind was HAPEX-MOBILHY (André et al. 1986), which took place in south-

* Current affiliation: ECMWF, Shinfield Park, Reading, Berkshire, United Kingdom.

Corresponding author address: Dr. J.-F. Mahfouf, European Centre for Medium-Range Weather Forecasts, Shinfield Park, Reading, Berkshire RG2 9AX, United Kingdom.

1995 American Meteorological Society

western France over crops and forested areas. Since HAPEX-MOBILHY, other experiments were undertaken over various ecosystems: grassland (FIFE 87-89), semidesert (EFEDA 91), savannah (HAPEX-SAHEL 92), and boreal forest (BOREAS 94).

In this general framework, Météo-France has developed a land surface scheme known as Interactions between Soil Biosphere Atmosphere (ISBA). This scheme described by Noilhan and Planton (1989) is based on the equations of the force-restore method of Deardorff (1977, 1978). Treatment of soil properties for heat and water transfer has been extended to the 11 soil types in the U.S. Department of Agriculture (USDA) classification. Treatment of the canopy layer has been simplified to avoid the numerical resolution of a specific foliage temperature. This scheme has been developed for both operational forecast and climate modeling requirements. This constraint explains why ISBA appear less sophisticated than SiB or BATS schemes. However, we believe that ISBA can capture the most important processes regulating heat and water exchanges in the soil–plant–atmosphere continuum. We also think that more sophisticated treatments lack knowledge of the large number of input parameters required on a global scale for the diversity of world ecosystems. This simple representation of the processes is also compatible with the "mosaic" approach of Koster and Suarez (1992) that permits an arbitrary number of vegetation types to coexist in a GCM grid square. Finally, the inclusion of a large number of prognostic variables in a land surface scheme causes the problem of initialization in operational mode.

The development strategy of ISBA has been described by Noilhan et al. (1993) and is briefly summarized here. An important study has been carried out to examine the behavior of this scheme at local scale over a wide range of surface types and atmospheric conditions. In these studies (Table 1), we have used the input parameters given by observations, the most important one being undoubtedly soil moisture content. Unknown physical parameters were set from values in the literature, while "scheme-dependent" parameters were tuned to reproduce observed energy and water balances. For example, Jacquemin and Noil (1990) have calibrated a dependency factor of the opy resistance with the saturation vapor deficit for niferous forest against HAPEX-MOBILHY d Mahfouf and Noilhan (1991) improved the repre tation of dew in the scheme for very dry soils, w Braud et al. (1993) demonstrated the importanc distinguishing roughness lengths for heat and mom tum in the EFEDA experiment. This local-scale e uation over varied ecosystems is an important asp for climate modeling where correspondence tables tween vegetation and soil types and parameters of scheme are required.

By including ISBA in the Météo-France mesos model PERIDOT, Bougeault et al. (1991a,b) h demonstrated its ability to reproduce atmospheric tures observed during clear sky periods of the HAPE MOBILHY experiment. Special emphasis has b placed on turbulent fluxes measured from airc (Noilhan et al. 1991). The model captured the c trasted Bowen ratio between the coniferous Les Lan forest and the surrounding crop areas. As a con quence, this mesoscale model has been used by Noil and Lacarrère (1995) as an integration tool for e mating the mean surface evaporation flux over the × 100 km HAPEX square. Noilhan and Lacar (1995) defined averaging procedures for vegetation soil properties to retrieve the average flux of the soscale model with a single column model represent the grid box of a GCM. The formal expression of surface evaporation flux remains the same and subgrid variability is introduced in the definition effective parameters.

In this paper, we describe the implementation of ISBA scheme within the Météo-France global clim model ARPEGE (Déqué et al. 1994). This study lows an initial work of Manzi and Planton (199 who included ISBA in a previous climate mo EMERAUDE. We show that the inclusion of scheme in a GCM takes advantage of both the v dation at local scale for the design of the scheme, c ibrations, and measurements of surface properties d ing HAPEX-type experiments to define the corresp

TABLE 1. Summary of the local evaluations of the ISBA scheme against field experiments.

Reference	Dataset	Timescale	Land cover
Noilhan and Planton (1989)	HAPEX-MOBILHY 86	clear sky days	crop/loam-sand
Jacquemin and Noilhan (1990)	HAPEX-MOBILHY 86	clear sky days	pine forest/sand
Mahfouf and Jacquemin (1989)	HAPEX-MOBILHY 86	rainy days	crop/loam-sand
Mahfouf (1990)	HAPEX-MOBILHY 86	months	crop/loam-sand
Noilhan and Mahfouf (1994)	HAPEX-MOBILHY 86	year	crop/loam-sand
Mahfouf and Noilhan (1991)	AVIGNON 84	week	bare soil/loam
Braud et al. (1993)	EFEDA 91	weeks	bare soil/loam
Germain (1991)	FIFE 87	clear sky days	grassland/loam
Manzi (1993)	ARME 84	year	tropical forest/loam
Manzi (1993)	ABRACOS 90	clear sky days	deforested clearing/l
Mahfouf (1994)	HAPEX-SAHEL 92	clear sky days	savannah/loam

dence table introduced hereafter, and averaging procedures deduced from mesoscale modeling to define effective surface parameters at the GCM grid scale. The methodology is rather original since generally, in climate modeling, surface properties are obtained from literature values and averaging procedures defined a priori.

The scheme is briefly described in section 2 with its specific modifications for climate modeling. Section 3 is concerned with the establishment of soil and vegetation maps on a global scale. The simulation of the present-day climate, with particular attention on near-surface parameters and on the hydrological cycle, is presented in section 5 after a description of the experimental design. Part II of this paper will show results from tropical deforestation experiments.

2. The numerical model

a. The land surface scheme

The ISBA scheme predicts the evolution of five prognostic variables for the surface temperature T_s, the mean surface temperature T_2, the surface volumetric water content w_g, the mean volumetric water content w_2, and the water amount of an interception reservoir W_r:

$$\frac{\partial T_s}{\partial t} = C_T(R_n - H - LE) - \frac{2\pi}{\tau_1}(T_s - T_2) \quad (1)$$

$$\frac{\partial T_2}{\partial t} = \frac{1}{\tau_1}(T_s - T_2) - \frac{2\pi}{\tau_2}(T_2 - T_c) \quad (2)$$

$$\frac{\partial w_s}{\partial t} = \frac{C_1}{\rho_w d_1}(P_g - E_g) - \frac{C_2}{\tau_1}(w_g - w_{geq}) \qquad 0 \leq w_g \leq w_{sat} \quad (3)$$

$$\frac{\partial w_2}{\partial t} = \frac{1}{\rho_w d_2}(P_g - E_g - E_{tr}) - \frac{C_3}{\tau_1}\max[0, (w_2 - w_{fc})] \quad 0 \leq w_2 \leq w_{sat} \quad (4)$$

$$\frac{\partial W_r}{\partial t} = \text{veg}P - E_r - R_r. \quad (5)$$

A list of symbols is given in appendix A. Some modifications to the initial proposal of Noilhan and Planton (1989) were applied for climate modeling purposes.

The mean surface temperature T_2 is restored toward a climatological deep temperature T_c updated with a time constant τ_2 of 20 days. The climatological temperature T_c is updated every month and has been obtained from the National Center for Atmospheric Research (NCAR) temperature climatology at 850 hPa by extrapolating to ground level. Damping and a phase lag with soil depth was obtained from a spectral analysis assuming constant thermal properties (Déqué et al. 1992). This term is only significant over continental areas during the polar night to avoid spurious drift toward too low temperatures produced by the radiative cooling of the surface. A more realistic treatment of deep soil heat transfers will be considered in future versions of ISBA by generalizing the force-restore method to the annual cycle as proposed by Dickinson (1988) and Jacobsen and Heise (1982).

The soil is defined to have a depth d_2 including the root zone. Soil water is characterized by three threshold values. The saturation water content (or porosity) w_{sat} is the maximum amount of water that a given soil can hold. The field capacity w_{fc} is the soil water content at which gravitational drainage effectively ceases. The wilting point w_{wilt} is the soil water content below which it is assumed that plants are unable to pump water from the root zone to stomatal cells. These three quantities depend upon soil texture. In the ISBA scheme, w_{sat} is estimated from Clapp and Hornberger (1978), w_{fc} corresponds to a hydraulic conductivity of 0.1 mm day^{-1} (Wetzel and Chang 1987), and w_{wilt} to a water potential of -15 bar. Evaporation is assumed to take place at the potential rate when soil moisture is between w_{fc} and w_{sat}, while transpiration ceases below w_{wilt}.

For short-term integrations, Noilhan and Planton (1989) have assumed no water flux at the lower boundary of the soil layer. For annual timescales, a deep drainage by gravity is added. Goutorbe et al. (1989) analyzed the evolution of soil moisture measured during 2 years at various locations within the experimental HAPEX-MOBILHY region. They showed that soil moisture content has an annual range between the field capacity and the wilting point. During the winter period, when precipitation exceeds evaporation, soil moisture remains at a constant value close to the field capacity implying, by conservation of water in the soil column, a water flux at the bottom. This subsurface runoff has been included by a restore term toward the field capacity in Eq. (4). The coefficient C_3 depends on soil texture and its estimation is presented in appendix B.

Runoff from the interception reservoir R_r has been modified to account for subgrid-scale variability of precipitation within a GCM grid box. Preliminary tests showed excessive interception loss over tropical forest with respect to observations. Over the Amazon forest during the ARME experiment, Shuttleworth (1988b) estimated the interception loss as being 20%–25% of the total evapotranspiration of the vegetation. This percentage was close to 80% in the initial simulations with the GCM (Benkiran and Cerisier 1993). As discussed by Dickinson (1989) and Shuttleworth and Dickinson (1989), this can have important consequences for the response of a GCM to tropical deforestation.

The drip from the foliage was previously calculated in ISBA by (Mahfouf and Jacquemin 1989)

$$R_r = \max\left(0, \frac{W_r - W_{r\max}}{\Delta t}\right), \quad (6)$$

where $W_{r\max}$ is the maximum amount of water stored on the canopy reservoir. This quantity is proportional to the vegetation density:

$$W_{r\max} = \gamma \, \mathrm{veg} LAI, \quad (7)$$

with $\gamma = 0.125$ resulting from a calibration using ARME data (Noilhan et al. 1993; Sellers et al. 1989).

By assuming an exponential distribution of precipitation (Eagleson et al. 1987), the drip from the interception reservoir can be written as (Shuttleworth 1988b; Dolman and Gregory 1992):

$$R_r = P_v \exp\left(-\mu \frac{W_r - W_{r\max}}{P_v \Delta t}\right). \quad (8)$$

The parameter μ represents the fraction of the grid cell area covered by rainfall, and P_v is the mean precipitation rate predicted by the GCM above the canopy within the grid cell. A study of Pitman et al. (1993) showed an important sensitivity of the partition of incident rainfall between runoff and evaporation to the distribution of precipitation with the BATS scheme. In a recent study, Eltahir and Bras (1993) proposed a method to estimate the parameter μ from a climatology of rainfall intensity. To simplify the approach, a constant value of 0.1, already chosen by Dolman and Gregory (1992), has been adopted.

As previously noted by Mahfouf and Jacquemin (1989), when Eq. (8) is used to represent runoff from the interception reservoir, $W_{r\max}$ is not anymore the maximum amount of water that the foliage can hold. It becomes a quantity equivalent to the field capacity for a soil: a threshold above which evaporation is potential. Since W_r can be greater than $W_{r\max}$, the fraction of wetted foliage is modified:

$$\delta = \min\left(1, \frac{W_r}{W_{r\max}}\right). \quad (9)$$

We have retained in Eq. (9) the formula of Rutter et al. (1971) instead of the one proposed by Deardorff (1978) in order to slow down the drying of the foliage (Mahfouf and Jacquemin 1989; Manzi and Planton 1994).

Since the surface temperature T_s is representative of both the vegetation and the soil surface, the thermal properties of these two media are averaged:

$$C_T = 1 \Big/ \left(\frac{1 - \mathrm{veg}}{C_G} + \frac{\mathrm{veg}}{C_v}\right). \quad (10)$$

The value representative of vegetation C_v is set to 2.10^{-5} J^{-1} m^2 K. This value is one order of magnitude higher than that of a soil C_G, in order to account for the reduction of the ground heat flux in the presence of a vegetation layer (low thermal inertia). We have chosen a lower value than in the proposal of Noilhan and Planton (1989), after Manzi and Planton (1994) demonstrated that for well-developed vegetation a heat storage term has to be taken into account. Moreover, it removes too cold nocturnal surface temperatures simulated over dense canopies (Giordani 1991).

The parameters C_G, C_1, C_2, and w_{geq} depend upon soil texture and soil moisture. They have been calibrated by Noilhan and Planton (1989) for the 11 soil types of the USDA textural classification using relationships for hydraulic conductivity and water potential proposed by Clapp and Hornberger (1978). The four quantities are expressed as functions (power fit) of w_g and w_2 and of parameters depending upon only soil texture: $C_{G\mathrm{sat}}$, $C_{2\mathrm{ref}}$, $C_{1\mathrm{sat}}$, a, b, and p. The dependence was tabulated for 11 soil types by Noilhan and Planton (1989). They are expressed by Noilhan and Lacarrère (1995) as continuous functions of the fraction of sand X_{sand} or clay X_{clay} in a given soil.

The vegetation is described by its horizontal density, veg, within each model grid box used for the partition of evaporation fluxes and for the estimation of averaged surface properties, its leaf area index LAI, and a minimum surface resistance to transpiration $R_{s\min}$. The roughness length Z_0, the albedo α, the emissivity ϵ, and the depth of the soil column d_2 are related both to the dominant vegetation and soil types.

The total evaporation flux is the sum of three components (evaporation from bare ground, foliage transpiration, and interception loss):

$$E = (1 - \mathrm{veg})\rho \frac{H_u(w_s) q_{\mathrm{sat}}(T_s) - q_a}{R_a(Z_0)} + \mathrm{veg}\rho\left[(1 - \delta)\frac{q_{\mathrm{sat}}(T_s) - q_a}{R_s(w_2) + R_a(Z_0)} + \delta \frac{q_{\mathrm{sat}}(T_s) - q_a}{R_a(Z_0)}\right] \quad (11)$$

b. The atmospheric part

The land surface scheme ISBA has been included in the Météo-France climate model ARPEGE (Version 1), which is an adaptation from the operational forecast model by Déqué et al. (1994).

The atmospheric model uses truncated spherical harmonics to represent variables in the horizontal and a hybrid coordinate for the vertical discretization. The chosen truncation is triangular (isotropic) up to wavenumber 42. The associated Gaussian grid for nonlinear and physics calculations has a resolution of 2.8°, following Hortal and Simmons (1991), a reduced Gaussian grid is adopted. The saving in computing time is about 20%, and although nonlinear terms are not totally free of aliasing, no significative degradation of the simulated climate have been noticed with respect to the full Gaussian grid. Each vertical is divided

TABLE 2. Correspondence table between vegetation types and parameters of the land surface scheme.

Vegetation type	d_{veg} (m)	α	Z_{0v} (m)	veg_{min}	veg_{max}	LAI_{min} ($m^2\ m^{-2}$)	LAI_{max} ($m^2\ m^{-2}$)	R_{smin} ($s\ m^{-1}$)
Crop	2.0	0.20	0.15	0.05	0.90	0.10	4.00	40
Short grass	1.5	0.20	0.02	0.85	0.85	1.00	1.00	40
Evergreen need-leaf tree	3.0	0.10	2.00	0.90	0.90	5.00	5.00	250
Deciduous need-leaf tree	1.0	0.11	2.00	0.90	0.90	0.10	5.00	250
Deciduous broad-leaf tree	3.0	0.12	2.00	0.90	0.90	0.10	5.00	250
Evergreen broad-leaf tree	3.0	0.12	4.00	0.99	0.99	6.00	6.00	250
Savannah	2.0	0.20	0.10	0.30	0.30	0.50	2.00	40
Tundra	1.0	0.16	0.05	0.50	0.50	0.50	2.00	150
Semidesert	1.0	0.25	0.05	0.10	0.10	0.50	0.50	150
Bog or marsh	1.0	0.12	0.05	0.60	0.60	4.00	4.00	150
Evergreen shrub	2.0	0.20	0.10	0.50	0.50	3.00	3.00	150
Deciduous shrub	2.0	0.20	0.10	0.50	0.50	0.50	3.00	150
Mixed woodland	2.0	0.12	2.00	0.90	0.90	3.00	5.00	250

layers with a high resolution in the lower troposphere to better describe the interactions between the surface and the planetary boundary layer. This resolution differs from the one chosen by Déqué et al. (1994).

The model has a comprehensive package of physical parameterizations. The radiation scheme is a modified and simplified version of the Ritter and Geleyn (1992) scheme. The radiative transfer equation is solved in two spectral intervals (one for the shortwave solar radiation and one for the longwave thermal radiation) by the δ-two-stream and adding methods. The effects of scattering, absorption, and emission by clouds, aerosols, and gases (H_2O, CO_2, O_3) are incorporated. The optical properties of clouds are related to cloud liquid water content, which is computed diagnostically by a method suggested by Betts and Harshvardan (1987). The radiation code is called every time step, thereby allowing accurate interactions with cloud cover and the diurnal cycle. Deep convection is modeled by a mass-flux scheme with detrainment (Bougeault 1985). A partial cloudiness is computed in each vertical layer with the assumption of random overlap between the layers. Stratiform cloudiness is a quadratic function of the relative humidity excess over a prescribed threshold relative humidity profile (Déqué et al. 1994). Convective cloudiness is diagnosed from convective precipitation using an empirical linear relation (Déqué et al. 1994). Stratiform precipitation forms when air becomes supersaturated. All condensed water is presumed to precipitate in one time step with possible evaporation in unsaturated layers below. Other parameterizations concern vertical diffusion represented by eddy diffusion coefficients (Louis 1979) and gravity wave drag. In this version, the photochemical parameterization of ozone is not active, nor is the ozone mixing ratio a prognostic variable. In the surface boundary layer, transfer coefficients are expressed using the similarity theory of Monin–Obukhov. Louis (1979) fitted the coefficients as a function of the Richardson number, in order to avoid the implicit calculation required when the Monin–Obukhov length is the stability parameter. Such formulation, revised by Louis et al. (1981), is introduced in the ARPEGE model. Mascart et al. (1995) have extended the polynomial fitting of Louis (1979) for the situations where roughness lengths for momentum Z_0 and for heat Z_{0H} are not equal. The importance of this distinction has been shown by various authors (Braud et al. 1993; Beljaars and Viterbo 1994). The ratio of the momentum to the heat roughness length Z_0/Z_{0H} is set to a constant value of 10 (Garratt and Hicks 1973).

3. Mapping of the surface parameters

a. Vegetation information

Vegetation types have been obtained from a global archive of land cover established by Wilson and Henderson-Sellers (1985). A set of 53 possible land cover types is available at a 1° horizontal resolution. Land cover types are given for primary vegetation covering more than 50% of the grid box and secondary vegetation, which occupies between 25 and 50% of the grid box. To reduce the difficulty associated with the definition of physical and biological properties of each vegetation type, Manzi and Planton (1994) gathered classes to obtain only 13 vegetation types. By including oceans, sea ice, and bare soil (deserts), 16 land cover types are retained. The parameters α, veg, R_{smin}, Z_0, LAI, and d_2 associated with each of the 13 vegetation types are listed in Table 2. We have used observed data and local calibrations for five land cover types: crops, grassland, tropical forest, savannah, and bare soil. The vegetation cover and the leaf area index include a seasonal cycle for crops, deciduous shrubs, and deciduous trees. For crops, we have followed the phenological evolution observed during HAPEX-MOBILHY (the dominant crop type was maize). For other types, we have imposed monthly values based on Dorman and Sellers (1989). When observed values were not available (tundra, marsh, shrubs), averaged estimates were

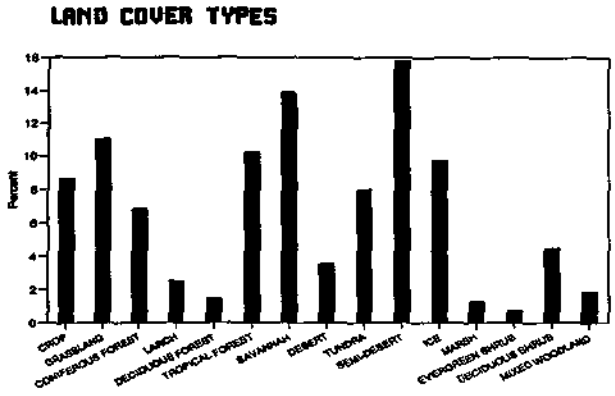

FIG. 1. Fraction of continents covered by the 15 selected land cover types on the T42 GCM grid deduced from the Wilson and Henderson-Sellers (1985) climatology.

taken from Dorman and Sellers (1989), Matthews (1985), and Pitman et al. (1991). The percentage of each vegetation over the globe is shown in Fig. 1. One can see that these "unknown" land cover types represent only a low percentage (less than 5%), except for tundra. The ratio $R_{s\min}/LAI$ has been estimated by an optimization procedure by Stewart (1988) for the Thetford pine forest (56 s m^{-1}), by Shuttleworth (1988b) for the Amazon rainforest (44 s m^{-1}), and by Stewart and Verma (1992) for the Konza prairie (40 s m^{-1}). Values in Table 2 are close to these estimates. The leaf area index LAI was measured during HAPEX-MOBILHY over maize, over the Amazon forest during ARME (Shuttleworth et al. 1984), and over savannah during HAPEX-SAHEL (Goutorbe et al. 1994). For grassland, FIFE estimates of LAI are between 1 and 2 (Stewart and Verma 1992). Forest albedos are deduced from measurements reported by Shuttleworth (1989). Albedos for crops and savannah were deduced from estimations of upward and downward solar radiation components measured during HAPEX. The roughness length has been taken equal to one-tenth of the vegetation height. For forest species, this value has been doubled to account for the displacement height that is not explicitly represented in the transfer coefficients of the surface boundary layer.

b. *Soil type information*

Two main sources were used for the soil information given by Wilson and Henderson-Sellers (1985) and Webb et al. (1991) at a 1° × 1° resolution. Their common origin is the FAO-UNESCO soil map of the world. Wilson and Henderson-Sellers (1985) gave three qualitative properties for soil color (light, medium, dark), soil texture (fine, medium, coarse), and drainage (free, medium, impeded). We have assigned for each color, a dry albedo value (Table 3) and for each drainage a soil depth d_{soil} (Table 4). Values for albedo adopted in Table 3 are somewhat larger than those proposed by Wilson and Henderson-Sellers (1985). The largest bare soil area is the Saharan desert, so we have chosen values giving the best agreement with satellite estimates from METEOSAT provided by Arino et al. (1991) over this region (0.35–0.40). Surface albedo is certainly the parameter that could be the most easily retrieved from satellite data, provided angular and atmospheric corrections are performed. One advantage of satellite retrieval is the ability to obtain different albedos at different locations over the globe for a given land cover. This is not possible when a specific albedo is assigned to a given ecosystem type. An indirect evaluation of the albedo maps will be given in the following section using clear sky planetary albedos from ERBE data. Textural information required by the ISBA scheme is the percentage of sand and clay within each grid box. Manzi and Planton (1994) assigned for each of the three textural classes of Wilson and Henderson-Sellers (1985) a percentage of silt, clay, and sand. Instead of introducing a supplementary correspondence table, we have used the fraction of sand and clay given by Webb et al. (1991) for a set of 15 horizons. Important differences have been found with the previous methodology. More differing soil types have been identified such as clayey soils over Amazonia and Eastern Australia, or sandy soils over Australia, the Sahel, and the Kalahari Desert (Fig. 2). The soil depth is also given by the Webb classification. However, in the ISBA scheme, this quantity is mostly related to the root zone of plants. Therefore, mapping of this parameter is deduced from the correspondence table of vegetation types. It has the advantage of being easy to modify for climate change studies. Spatial distribution obtained this way is well correlated with the soil depth map of Webb et al. (1991). Deep soils are associated with forest ecosystems except over deciduous need-leaf trees (larch) in Siberia where we have reduced the initial value of 3 to 1 m to match poor soil depth noticed in this region by Webb et al. (1991).

TABLE 3. Bare soil albedo for the three soil colors given by the Wilson and Henderson-Sellers (1985) classification.

Soil color	α_{soil}
light	0.40
medium	0.30
dark	0.20

TABLE 4. Soil depth for three soil drainage categories given by the Wilson and Henderson-Sellers (1985) classification.

Soil drainage	d_{soil}
rapid	1.00
poor	0.50
impeded	0.10

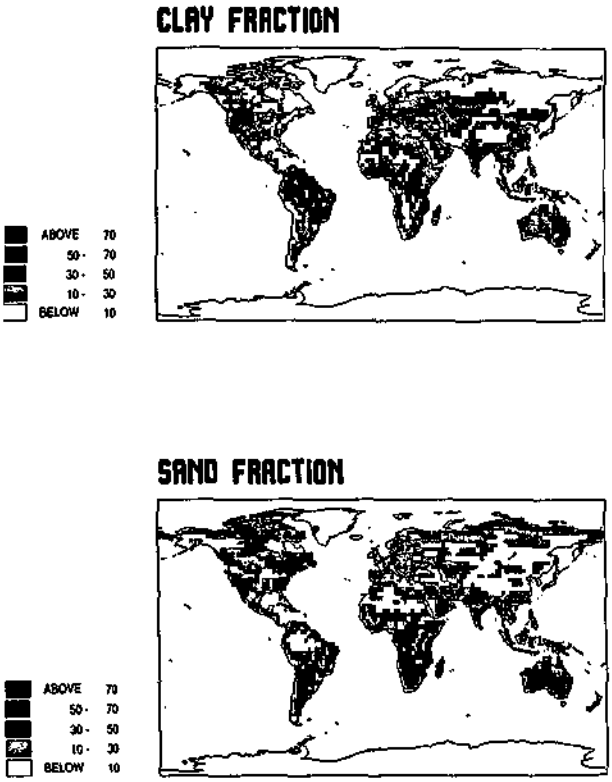

FIG. 2. Maps of the percentage of clay and sand on the T42 GCM grid deduced from the Webb et al. (1991) climatology.

c. Blended properties

A given surface property φ (veg, LAI, α) is averaged from its values for the dominant vegetation type φ_d and for the secondary vegetation type φ_s by

$$\varphi = 0.75\varphi_d + 0.25\varphi_s. \tag{12}$$

The roughness length associated with land cover is given by

$$Z_{0v} = 0.75 \frac{Z_{0vd}\,\mathrm{veg}_d}{\mathrm{veg}_{d\max}} + 0.25 \frac{Z_{0vs}\,\mathrm{veg}_s}{\mathrm{veg}_{s\max}}. \tag{13}$$

The total roughness length including the contribution of subgrid scale orography Z_{0rel} equals

$$Z_0 = \sqrt{Z_{0v}^2 + Z_{0rel}^2}. \tag{14}$$

The total albedo is

$$\alpha = \mathrm{veg}\,\alpha_{\mathrm{veg}} + (1 - \mathrm{veg})\alpha_{\mathrm{soil}}. \tag{15}$$

The depth d_2 of the active soil layer is obtained as the maximum of the vegetation root depth d_{veg} and the soil column depth d_{soil}:

$$d_2 = \max(d_{\mathrm{veg}}, d_{\mathrm{soil}}). \tag{16}$$

The emissivity ϵ is specified from CLIMAP data (Déqué et al. 1992).

d. Averaged properties

Noilhan and Lacarrère (1995) defined operators to transfer the land surface properties from a fine grid (here 1° × 1°) to a coarser grid (here T42). The underlying idea is to average quantities that are pseudo-linear with respect to the surface fluxes. If the percentage of land cover type i within a coarse grid is f_i, the mean property φ is given by

$$\varphi = \sum_{i=1}^{N} f_i\varphi_i, \tag{17}$$

with φ = veg, α, LAI, d_2, $\ln(Z_0)$, $1/R_{s\min}$, X_{sand}, and X_{clay}. The other approach for dealing with the problem of spatial heterogeneity is to estimate the flux of each patchiness and then estimate the total area flux as the sum of each component (Koster and Suarez 1992; Ducoudré et al. 1993).

The continuous formulation of soil thermohydric properties devised by Noilhan and Lacarrère (1995) allows for an easier averaging procedure than on the parameters themselves due to weaker nonlinearities.

4. Experimental design

A 3-yr control experiment has been performed forced with climatological sea surface temperatures and sea-ice extents obtained from COLA/CAC and averaged over the AMIP period 1979–1988. The simulation begins on 1 September 1979 from a European Centre for Medium-Range Weather Forecasts (ECMWF) analysis interpolated and truncated to the model resolution. Soil moisture was initialized using an indirect climatology of soil moisture availability ψ based on observations of temperature and dewpoint temperature at 850 hPa from NCAR climatology. Surface relative humidity is related to soil moisture using an empirical relationship (Déqué et al. 1992). To have water contents consistent with soil depth d_2 and soil texture, we have scaled the parameter ψ by the permanent wilting point w_{wilt} and the field capacity w_{fc}. The water depth W for a grid box characterized by a moisture availability ψ is given by

$$W = [(w_{fc} - w_{\mathrm{wilt}})\psi + w_{\mathrm{wilt}}]d_2. \tag{18}$$

The geographical distribution of soil moisture obtained this way agrees with the Mintz and Serafini (1992) climatology. It will be shown in the results that over specific regions, the surface scheme remembers the initial soil moisture for long periods of time, and hence the initialization is important.

Screen-level temperature, precipitation, surface evaporation, runoff, and clear sky planetary albedo have been examined and are compared with observed climatologies. Regional analyses have also been performed to check the behavior of the model over different regions following the methodology of Garratt et al. (1993). Special emphasis is placed on the Amazon

region since measurements from ARME are available (Shuttleworth et al. 1984).

Manzi and Planton (1994) have already compared results produced with and without the ISBA scheme in the former Météo-France climate GCM where an intensification of the hydrological cycle and a cooling of the surface was noticed. The general pattern of model errors on the global scale has not been modified by the ISBA scheme. However, some improvements were noticed at regional scale. Over Amazonia, results were found to be more realistic with the new scheme during the dry season.

5. Results

Our attention is focused on parameters that are of importance for continental surfaces either as forcing terms (precipitation, radiation) or as by-products of the land surface scheme (evaporation). We will try to capture the spatio-temporal structure of these fields by examining them in different ways using various types of diagnostics.

a. Global analysis

1) CLEAR SKY PLANETARY ALBEDO

The realism of the land cover imposed at the lower boundary of our model cannot be easily evaluated on the global scale except for the surface albedo where remote-sensed observations are available. One manner to verify this field is to compare clear sky planetary albedo against cloudless scenes from satellite data. This comparison is presented in Fig. 3 for each land cover category of the continental surfaces. Averaged model values for 16 types are compared with the satellite counterpart derived from the Earth Radiation Budget Experiment (ERBE). We have chosen the month of July for the comparison in order to reduce the influence of snow cover. Satellite data are averaged over four Julys (1985–1988). Possible differences may not be due solely to the surface, since top of the atmosphere albedos also include an atmospheric contribution. Also, the sampling method of clear sky pixels is different for the model and the satellite data. The model computes clear sky radiative fluxes every 3 h in the course of the integration, while for the satellite, monthly averages are performed only with observed clear sky scenes [respectively, methods II and I in the terminology proposed by Cess and Potter (1987)]. Figure 3 reveals an agreement of the model data with the satellite observations. The model captures the high albedos above 50% over ice caps, the large values associated with desert and semidesert areas near 25%, and the low albedos (14%) characterizing tropical forests. Crops and grassland surfaces have slightly higher albedos than observed with an overestimation around 10% in relative. Savannah albedo is overestimated and this could be important because this surface type represents 13% of the

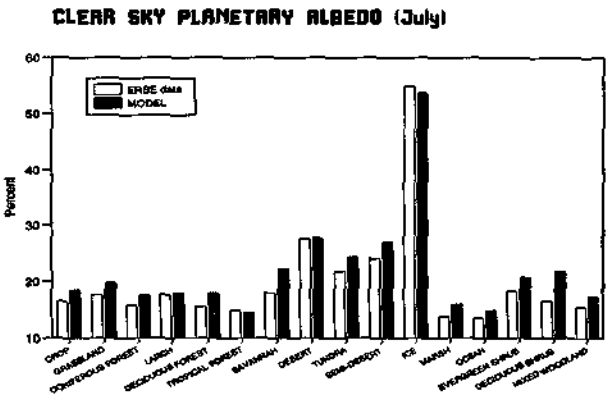

FIG. 3. Comparison of the modeled clear sky planetary albedo with ERBE data in July for each land cover category.

continental surfaces of the world. The averaged albedo over savannah is 22% instead of 18%. For other vegetation types such as deciduous forest or marsh, differences are less critical since their surface coverage is less than 5% of the globe (Fig. 1). Surface albedo and vegetation cover for savannah have been calibrated against local measurements from HAPEX-SAHEL. However, this vegetation type is also present over a large fraction of South Africa and South America with apparently lower values. This reveals a weakness of the mapping method, which assumes that a given vegetation type has the same albedo over all the world. One can see that the model captures the contrasting albedos of the various land covers but often slightly overestimated. This defect comes principally from having a too high albedo over bare light soils. Selected values in Table 3 are well fitted for Saharan desert but lead to a positive bias over regions where the contribution of bare soil to total albedo is non-negligible.

2) PRECIPITATION AND AIR TEMPERATURE

Rainfall is an input to the land surface hydrology scheme and therefore strongly drives its behavior. The global geographical distribution of precipitation simulated by the model can be compared with the climatology of Legates and Willmott (1990a,b) for the annual mean quantities in Fig. 4 (seasonal evaluation is discussed for regional analyses). The large-scale characteristics of precipitation are reasonably simulated. The intense equatorial belt along the ITCZ with three maxima located over continents (South America, Africa, Indonesia) are present. The intensity is somewhat underestimated in the eastern equatorial Pacific and over South America. The South Pacific convergence zone is simulated. Over Southeast Asia, a maximum is displaced westward near the Bay of Bengal. Midlatitude storm track maxima over the oceans are also modeled. Over the North Atlantic and North Pacific, the model poorly simulates the enhanced precip-

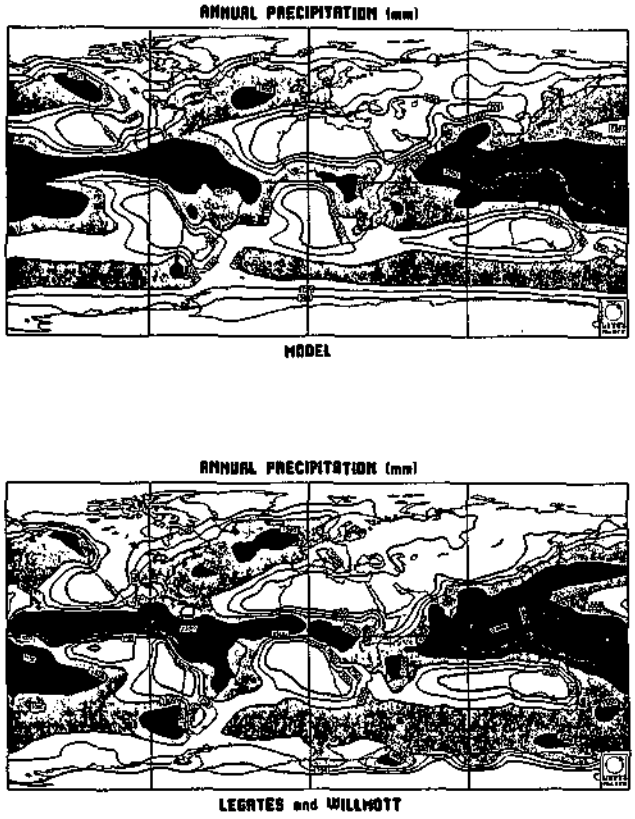

FIG. 4. Mean annual distribution of precipitation from the atmospheric model (top) and the observed data of Legates and Willmott (1990a; bottom).

itation over warm ocean currents, inducing too low rainfall rates along the eastern coast of North America. Siberian rainfall is substantially overestimated. Dry areas above deserts, subtropical oceans, and polar regions are in agreement with the climatology both for spatial extent and intensity. As already noted by Manzi and Planton (1994), the general pattern of model errors on the global scale is not sensitive to the new land surface scheme ISBA (Benkiran and Cerisier 1993).

The mean annual surface air temperature simulated by ARPEGE is shown in Fig. 5 together with the climatology developed by Legates and Willmott (1990b). Lower than observed temperatures are found over most terrestrial regions, for instance North Africa, Venezuela, and Greenland. Two possible reasons can be identified: excessive surface evaporation and insufficient downward radiation at the surface. Over mountainous regions (Tibetan Plateau, Rockies, Andes), underestimation possibly comes from an inconsistency in the representation of surface elevation between the model and reality.

The precipitation and air temperature fields can be combined to constitute the climate classification proposed by Köppen (1923). The Köppen climate classification is based on annual cycles of temperature and precipitation. A set of 11 climate zones is identified based on simple criteria for the minima and maxima of these two fields. The way the classification is obtained is summarized in Table 5. The Köppen classification is applied to model outputs and to the climatological observed air temperature (Legates and Willmott 1990b) and precipitation (Legates and Willmott 1990b). The fraction of continents covered by different climate zones is presented in Fig. 6 for the observations and the model simulation. The simulated classes match well with the observed ones. Large differences can be noticed for the tropical savannah climate (Aw) underestimated by a factor of 2, whereas the inverse is noticed for the warm climate with dry winter (Cw). Examination of the geographical distribution indicates that the model produces a shift of climate zones Aw and Af to the climate zone Cw over South Africa. This is a consequence of a too cold minimum temperature and too much rainfall in the summer season. Over Argentina, climate zone Dw is replaced by Cw, by having a too cold minimum temperature. The climate zone Cf present in the climatology over western Europe and the eastern United States is underestimated as being almost absent of the United States. Climate zone Df located over Canada and the Eurasian continent ex-

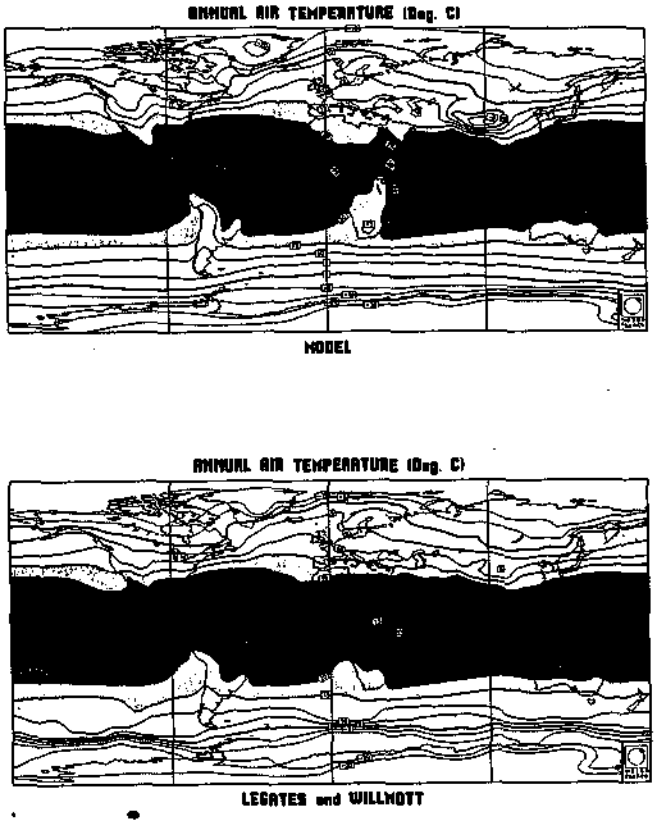

FIG. 5. Mean annual distribution of surface air temperature from the atmospheric model (top) and the observed data of Legates and Willmott (1990b; bottom).

tends too far south over the Gobi Desert due to excessive precipitation, at the expense of the BS and BW climates. Most of Greenland is colder than 0°C in the model enhancing climate zone EF and reducing ET.

3) Runoff

Precipitation is the most documented component of the surface hydrological budget, whereas the two other fluxes (evaporation and runoff) are less accurately known. It also seems important to know whether water input over land is correctly partitioned into evaporation and runoff by the surface hydrology scheme, even if available data have to be considered as guidelines only. Continental runoff can be obtained over drainage basins by measuring the flow rate of the world's major rivers. The approach proposed by Russell and Miller (1990) for the GISS GCM has also been applied by Dümenil and Todini (1992) to the ECHAM model. In the latter case, a horizontal advection scheme of underground water flow is introduced for an evaluation of the freshwater flow required in atmosphere–ocean coupled runs. In this case, a comparison of the observed and modeled runoff can be done on a monthly time basis because the delay between instantaneous runoff and river flow modification is taken into account. Without this horizontal transport, comparison between calculated runoff and river flow is relevant only on an annual mean basis. We have selected a set of 15 river drainage basins over the world. Model grid boxes were chosen in accordance with Dümenil and Todini (1992) estimates. Comparison of observed values given by Milliman and Meade (1983) and model-generated runoff is presented in Fig. 7. Runoff from the Amazon is one third of the observed value. In the southern part of this continent, runoff from La Plata River is correct. Over the North American continent, the modeled runoff is in good agreement with observed values for the McKenzie and the St. Lawrence rivers. The model generates negligible runoff for the Mississippi River (29 mm instead of 180 mm). Over high latitudes in Asia, runoff is too high for the four rivers concerned (Ob, Lena, Amur, and Yenesei). Over India, although the model estimate is quite large for the Brahamaputra River, this runoff is still too low by 100 mm. The same deficiency appears for the Indus River and in China for the Yangtze River and Indus River. In Africa, runoff is slightly underpredicted for two of the three major river basins (Zambesi, Niger) and is well simulated for the Zaire River.

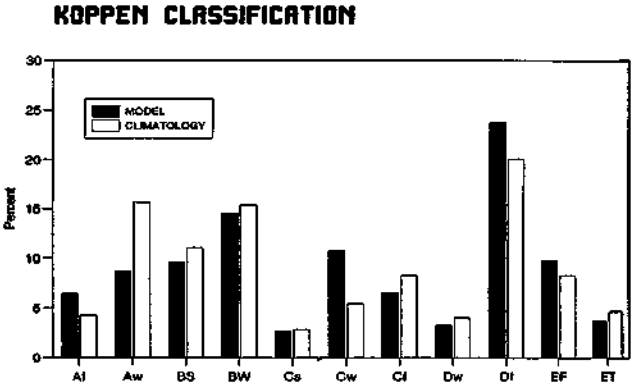

FIG. 6. Fraction of continents covered by the different Köppen climate zones for observations (Legates and Willmott 1990a,b) and the model simulation.

TABLE 5. Climate classification from Köppen. Here t_{min} and t_{max} represent the monthly mean temperature of the coldest and warmest months, respectively: $\bar{r}$, r_{min}, and r_{max} present the annual mean precipitation and monthly mean precipitation of the driest and wettest months, respectively; and r_{smin}, r_{smax}, r_{wmin}, and r_{wmax} are the precipitation of the driest summer month, the precipitation of the wettest summer month, the precipitation of the driest winter month, and the precipitation of the wettest winter month, respectively. Here r_d is a threshold precipitation that depends on the annual mean temperature $\bar{t}$ and the annual cycle of precipitation: $r_d = 2\bar{t}$ if at least 70% of the annual precipitation occurs in winter, $r_d = 2\bar{t} + 28$ if at least 70% of the annual cycle precipitation occurs in summer, and $r_d = 2\bar{t} + 14$ otherwise.

Type	Subtype	Name	Criterion
A		tropical rainy climates	$t_{min} \geq 18$°C
	Af	tropical rainforest climate	$r_{min} \geq 6$ cm month^{-1}
	Aw	tropical savannah climate	$r_{min} < 6$ cm month^{-1}
B		dry climates	$\bar{r} \geq r_d$
	BS	steppe climate	$\bar{r} \geq r_d/2$
	BW	desert climate	$\bar{r} < r_d/2$
C		humid mesothermal climates	-3°C $\leq t_{min} < 18$°C
	Cs	warm climate with dry summer	$r_{wmax} \geq 3.r_{smin}$
	Cw	warm climate with dry winter	$r_{smax} \geq 10.r_{wmin}$
	Cf	humid temperature climate	$r_{smax} < 10.r_{wmin}$ and $r_{wmax} < 3.r_{smin}$
D		humid microthermal climates	$t_{min} < 3$°C and $t_{max} \geq 10$°C
	Dw	cold climate with dry winter	$r_{wmax} \geq 10.r_{wmin}$
	Df	cold climate with moist winter	$r_{wmax} < 10.r_{wmin}$
E		polar climates	$t_{max} < 10$°C
	ET	tundra climate	0°C $\leq t_{max} < 10$°C
	EF	permafrost	$t_{max} < 0$°C

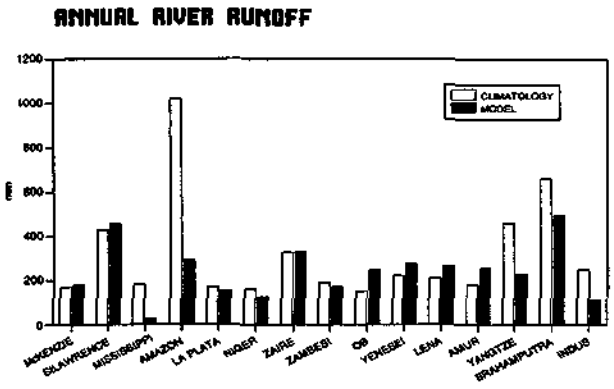

FIG. 7. Mean annual runoff for the world's largest rivers. Comparison between modeled runoff and observed runoff of Milliman and Maede (1983).

In general, runoff anomalies are consistent with discrepancies previously noticed in the modeled precipitation. At high latitudes, precipitation is overestimated inducing too much runoff in the model. An excess in precipitation generates too large evaporation rates through soil moistening, thereby reducing the runoff bias. Over Canada, these too large values compensate to produce runoff amounts close to observations. However, overestimation of precipitation is reflected in runoff for rivers located in Siberia. For equatorial and tropical regions, except in Amazonia, runoff is underestimated despite precipitation close or higher than climatology. Rainfall rate is high in these regions (above 1000 mm yr^{-1}), saturating soils and thereby producing excessive potential evaporation. One way to increase runoff at the expense of evaporation would be the introduction of subgrid scale variability of soil infiltration (Shuttleworth 1988a) or soil water holding capacity (Dümenil and Todini 1992). These techniques allow runoff to occur before a complete saturation of the soil water reservoirs. The behavior for the Amazon is different due to a rainfall underestimation by the model. However, the introduction a deep gravitational drainage in the evolution of the mean volumetric water content has significantly increased runoff in these regions compared with previous simulations (Cerisier and Benkiran 1993). Runoff predictions by bucket type models for these regions are generally acceptable, provided precipitation is correctly simulated. This can be explained by their small water-holding capacity (Mintz and Serafini 1992; Russell and Miller 1990). Behavior of the Mississippi Basin is atypical with excessive evaporation and too low rainfall rates.

b. *Regional analysis*

In this section, analyses are presented for five contrasting regions (Eurasia, eastern United States, Australia, Central Sahel, Amazonia) already studied by Garratt et al. (1993) in GCM evaluations. These selected zones are displayed in Fig. 8. Each zone encompasses about 40 model grid points. Model variables are compared with various climatologies for screen-level temperature (Legates and Willmott 1990b), precipitation (Legates and Willmott 1990a), cloudiness (ISCCP data), soil moisture and surface evaporation (Mintz and Serafini 1992), and net radiation (Henning 1989). A rigorous comparison with Mintz and Serafini (1992) should be made with caution because their result is based on a simple water budget model driven by the observed temperature and precipitation. Since Part II of this paper will examine tropical deforestation, the analysis over Amazonia will be emphasized where local measurements from the ARME field study are also available (Shuttleworth et al. 1984). We compare monthly mean values averaged over the 3 years of integration except for soil moisture where the evolution over the whole period reveals interesting features. The climatology of Mintz and Serafini (1992) provides normalized amounts of soil moisture between zero and one. In the model outputs, the mean volumetric water content w_2 is combined with the field capacity w_{fc} and the wilting point w_{wilt} to create the following dimensionless variable ψ:

$$\psi = \frac{w_2 - w_{wilt}}{w_{fc} - w_{wilt}}. \tag{19}$$

Figure 9 reveals that over Amazonia, with a large water input, less than 1 year is needed to reach a quasi-equilibrium state. The seasonal cycle follows the climatology with maximum amounts close to the field capacity in the rainy season. The introduction of a subsurface gravitational percolation with an e-folding time of a few days precludes values above the field capacity on the monthly averages. Over Eurasia, where the annual precipitation is important, equilibrium is also reached by the end of the first year. The same is observed for the eastern United States although with a drier soil than the climatology. For desertic areas (Africa, Australia), even after three years of integration a decreasing trend persists, which indicates that the atmosphere is

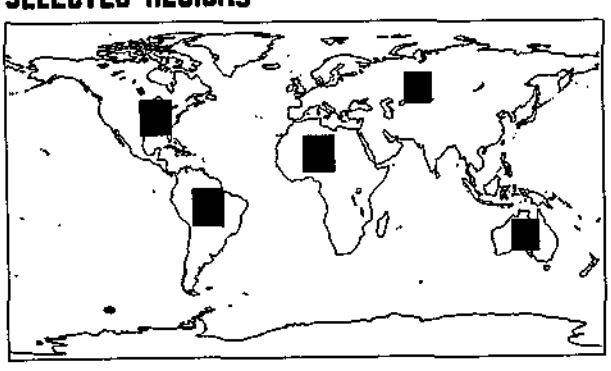

FIG. 8. Location of the five selected continental regions.

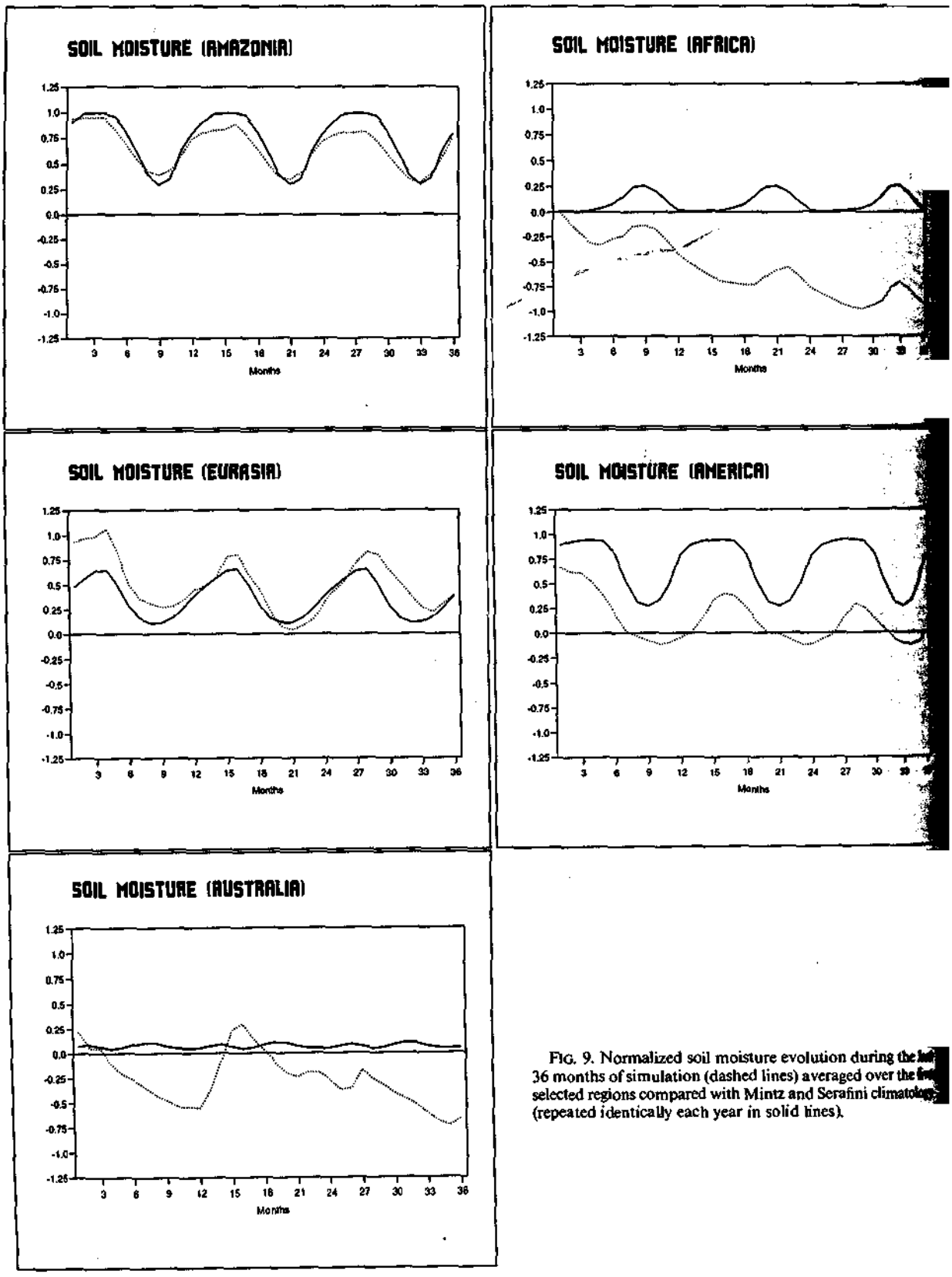

FIG. 9. Normalized soil moisture evolution during the last 36 months of simulation (dashed lines) averaged over the first selected regions compared with Mintz and Serafini climatology (repeated identically each year in solid lines).

still removing water from the soil. The normalized parameter ψ is negative in these regions since soil moisture is below the wilting point (which was the initial value as described in section 4). Several conclusions can be drawn from this behavior. Initialization of soil moisture is important even for climate modeling as pointed out by Serafini (1990). Its importance is particularly pronounced over regions where the water input is weak and where bare soil evaporation dominates (i.e., desertic areas). For these situations, the memory of the initial state can last for several years since bare soil evaporation manages only small amounts of water within the superficial reservoir. Another feature is that the wilting point is a useful lower bound of soil moisture only in the presence of vegetation. Over bare soil, soil moisture can drop far below this value. In the future, the soil moisture initialization procedure of our model will include the vegetation fraction to provide a better

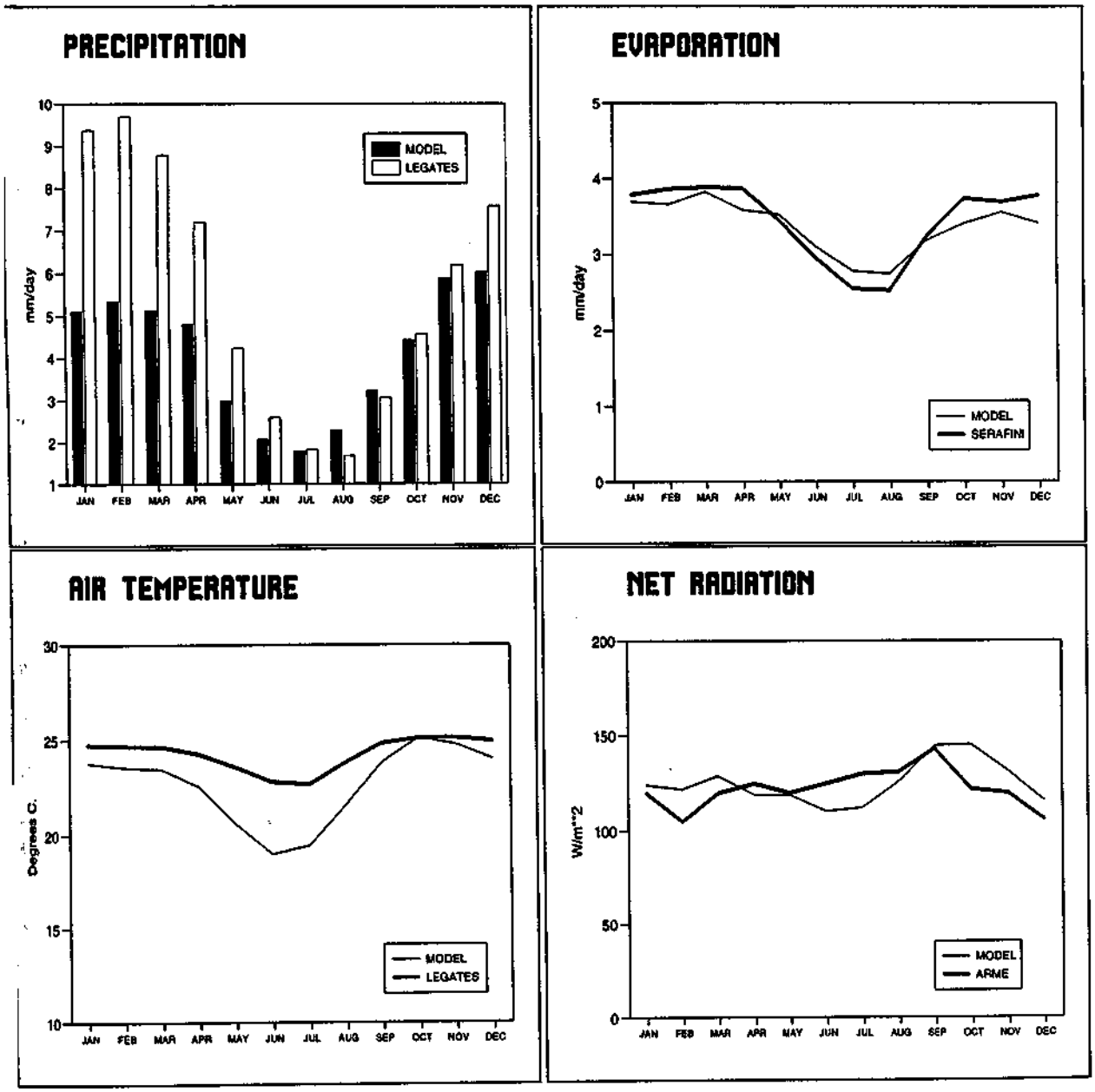

FIG. 10. Mean seasonal cycle of precipitation, surface evaporation, surface air temperature, and net radiation over the Amazon region. Modeled precipitation is compared with Legates and Willmott (1990a) values. Modeled evaporation is compared with Mintz and Serafini (1992) values. Modeled surface air temperature is compared with Legates and Willmott (1990b) values. Modeled net radiation is compared with ARME data from Shuttleworth et al. (1984).

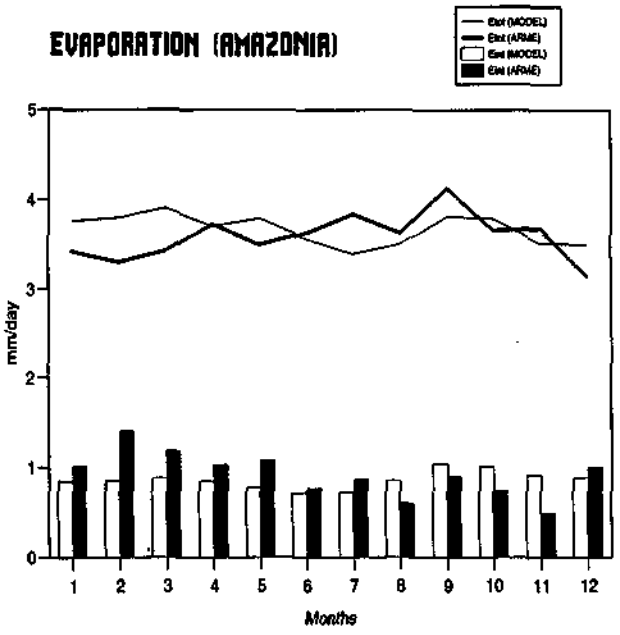

FIG. 11. Mean seasonal cycle of total evaporation and interception loss over the Amazon forest. Simulated cycles are compared with the ARME data from Shuttleworth et al. (1984) and Shuttleworth (1988b).

first guess over desert areas (Manzi 1993). Our major concern in Part II is tropical regions where the presence of vegetation and large precipitation amounts remove this problem. A study with a focus on semiarid regions has to be aware of this problem. All these findings are in agreement with sensitivity studies undertaken in stand-alone mode with ISBA in the PILPS program (Mahfouf and Noilhan 1993).

Over Amazonia, the seasonal cycle of precipitation is in phase with the climatology, but an important underestimation by a factor two is noticed during the first 4 months of the year (Fig. 10). For the remaining part of the year, the minimum corresponding to the dry season is well reproduced, as is the initial phase of the rainy season (September–December). Despite this weakness in precipitation, evaporation is large during the wet season with values close to the climatology. Evaporation is not limited by the surface (it rains enough in the model to be close to the field capacity) but by the available radiative energy. A decrease in evaporation is noticed in winter (JJA), which is also evident in the climatology. Decrease in evaporation during the dry season visible in Fig. 10 comes from the fact that the selected region shown in Fig. 8 encompasses not only tropical forest but also tall grass, having a lower water holding capacity. Since interception loss was measured during this field campaign, we have reported this component of evaporation in Fig. 11 to show that subgrid-scale variability of precipitation for canopy drainage leads to a prediction of the model close to measurements. Measurements exhibit a decreasing trend during the course of the year, while interception loss from the model follows the seasonal cycle of precipitation with minimum values in June–July. Evaporation computed by the model, when averaged over the Amazon forest as in Fig. 11, shows a behavior similar to the seasonal cycle presented by Shuttleworth (1988b) (almost constant rate around 3.7 mm day^{-1}). The agreement for evaporation is not an artifact of two opposite defects. The net radiation computed by the model is close to the one measured during ARME. The seasonal cycle has a weak amplitude around 130 W m^{-2} (Fig. 10). We can conclude that over this region, management of land surface processes is consistent with the available observations. This is a necessary condition in order to have some confidence in deforestation experiments described hereafter. Screen-level temperature maxima agree reasonably with observed climatology whereas minima are too low by 3 K. Surface albedos for the five regions are displayed in Table 6, indicating that over Amazonia, this parameter does not explain observed departures from the climatology. Thus, we suspect an underestimation of the downward net radiation, compatible with the fact that net radiation is close to climatology. A comparison with radiative measurements collected during ARME reveals that net downward radiation is underestimated by 40 W m^{-2} during the JJA period. More precisely, solar radiation is larger than observed (230 W m^{-2} instead of 180 W m^{-2}), while thermal downward radiation is too low by 90 W m^{-2}.

All results discussed hereafter are displayed in Tables 7 and 8. Over Africa, the contrasting precipitation regimes between JJA and DJF are reasonably simulated by the model. Winter evaporation, although very weak, is larger than the climatology due to the problem of soil moisture initialization previously mentioned. Over Eurasia, precipitation is always larger than climatology by about 1 mm day^{-1} with a direct consequence on evaporation principally during summer. The precipitation is underestimated during the whole year for the North America region with differences reaching 2 mm day^{-1} in winter. Evaporation is reasonable in summer, whereas in winter the net radiation is too large thereby enhancing water losses by the soil. Finally, the agreement is good over Australia both for precipitation and evaporation.

Important differences can be noticed for air temperature between modeled quantities and observed

TABLE 6. Surface albedo over selected regions from various sources.

Surface albedo	Amazonia	Africa	Eurasia	America	Australia
ISBA	0.15	0.32	0.23	0.19	0.31
HENNING	0.15	0.26	0.22	0.18	0.26
DORMAN-SELLERS	0.14	0.25	0.19	0.17	0.26
MATTHEWS	0.13	0.25	0.19	0.15	0.22

TABLE 7. Mean values of air temperature, precipitation, evaporation, net radiation and cloudiness for the period June–July–August over selected regions. Modeled values are compared with different climatologies.

Variable	Amazonia	Africa	Eurasia	America	Australia
Air temperature-Model (°C)	20.0	27.3	17.9	27.5	11.2
Air temperature-Legates (°C)	23.1	30.3	18.8	24.1	15.4
Precipitation-Model (mm day^{-1})	2.05	2.20	2.13	2.61	0.10
Precipitation-Legates (mm day^{-1})	2.03	2.51	1.56	3.56	0.41
Evaporation-Model (mm day^{-1})	2.87	1.92	2.67	3.36	0.35
Evaporation-Serafini (mm day^{-1})	2.67	1.80	1.94	3.96	0.54
Net radiation-Model (W m^{-2})	112	109	124	171	20
Net radiation-Henning (W m^{-2})	82	120	128	158	29
Cloudiness-Model (%)	43.1	39.8	43.9	35.3	17.5
Cloudiness-ISCCP (%)	42.6	31.1	49.5	50.1	21.1

ones. Over Africa, winter temperatures are underestimated by 5 K. A possible explanation is that the net radiative energy is too weak at the surface over this region. This effect is not found in the net radiation due to a compensation by weaker thermal losses from the surface. The same is true for Australia during the winter season. Sensitivity experiments with surface albedos reveal that values over Australia are somewhat overestimated and that reducing their values from 0.32 to 0.25 removes this cold bias (Mahdaoui 1994). Over the Sahel, the behavior is quite different. A reduction in surface albedo increases surface temperature by only 2 K, but unrealistically increases precipitation through a Charney-type feedback (Charney et al. 1977). The origin of this problem certainly lies in the radiative code. The use of the Surface Radiation Budget Global dataset compiled by the World Climate Research Programme (WCRP) and the National Aeronautics and Space Administration (NASA) would be helpful to go deeper in this direction. Over North America, the maximum temperature is overestimated by 3 K due to a too low cloud cover. Minima over Eurasia are too high by an enhancement in the greenhouse effect of clouds (cloud cover being 85% instead of 46%). The fact that snow thermal properties are not introduced in the global thermal coefficient C_T of the surface may also contribute to this warm bias.

6. Conclusions

In this paper, the methodology developed to implement an improved land surface scheme ISBA (Noilhan and Planton 1989) within the Météo-France climate model ARPEGE (Déqué et al. 1994) has been presented. The methodology is based on local validations over various ecosystems to establish correspondence tables between vegetation types and scheme parameters, and on mesoscale modeling to define grid-scale averaging procedures for scheme parameters. We have brought some modifications from the previous work of Manzi and Planton (1994) and Benkiran and Cerisier (1993). The proposal of Shuttleworth (1988a) has been used to account for precipitation spatial variability within the GCM grid box in estimating the canopy drainage. An additional term, representing subsurface gravitational drainage has been incorporated in the prognostic equation of the mean volumetric water content. Different roughness lengths are used for momentum and heat to compute turbulent transfers in the surface boundary layer. The correspondence table was modified to better match previous local calibrations. We used the recent soil climatology from Webb et al. (1991) giving explicitly the percentage of sand, loam, and clay at a 1° × 1° resolution. The last modification, with respect to the description of the ARPEGE model given by Déqué et al. (1994), has been

TABLE 8. As in Table 7 but for the period December–January–February.

Variable	Amazonia	Africa	Eurasia	America	Australia
Air temperature-Model (°C)	23.8	15.0	−11.4	2.2	27.8
Air temperature-Legates (°C)	24.8	20.4	−14.9	2.8	27.9
Precipitation-Model (mm day^{-1})	5.50	0.03	1.60	1.07	1.80
Precipitation-Legates (mm day^{-1})	9.00	0.05	1.25	2.69	1.78
Evaporation-Model (mm day^{-1})	3.58	0.60	0.21	0.74	1.72
Evaporation-Serafini (mm day^{-1})	3.81	0.19	0.00	0.24	1.72
Net radiation-Model (W m^{-2})	124	43	−9	10	133
Net radiation-Henning (W m^{-2})	123	37	−15	10	148
Cloudiness-Model (%)	86.4	22.7	86.5	56.6	27.2
Cloudiness-ISCCP (%)	83.7	21.3	44.7	56.8	46.2

the increase of the vertical resolution in the troposphere at the expense of stratospheric resolution.

The evaluation of a 3-yr integration for the present-day climate has focused on the hydrological cycle. Water management by the surface scheme is, in general, realistic, and most of the identified problems come from the hydrological forcing (precipitation) and from the radiative forcing (cloudiness, net solar radiation).

Future improvements will concern the mapping of surface albedo using satellite data to better distinguish bare soil surfaces at different locations of the globe, initialization of soil moisture to reduce the spinup time of the model and the representation of soil heat transfer by generalizing the force-restore method to the annual cycle. The seasonal cycle of the vegetation biomass (veg, *LAI*) will be improved by performing statistical regressions with global vegetation indexes from NOAA/AVHRR remote sensing data (Mahdaoui 1994). The inclusion of subgrid variability in convective precipitation for soil surface infiltration would likely remove part of the negative bias noticed in runoff over tropical regions. This first analysis will be completed by an evaluation of the surface radiative budget, since the first assessment with ARME data indicates that the radiative scheme seems to overpredict solar radiation and underpredict longwave thermal radiation at the surface. Available observed data on surface radiative fluxes are given from field experiments such as FIFE and from the first WCRP Surface Radiation Budget Global datasets. Improvements in other physical parameterizations (partial cloudiness and deep convection principally) of the model could lead to a better representation of land surface processes.

Acknowledgments. The authors would like to thank various students from the Ecole Nationale de la Météorologie for their important contribution in coding the ISBA scheme and performing preliminary evaluations, particularly P. Le Moigne, W. Maurel, N. Cerisier, C. Benkiran, and F. El Mahdaoui. We would also like to thank Dr. D. Stephenson for his careful reading of the manuscript. This work was supported by grants from the Commission of the European Communities and from the Programme National d'Etude de la Dynamique du Climat.

APPENDIX A

List of Symbols

b	slope of the retention curve
C_G	soil thermal coefficient
C_v	vegetation thermal coefficient
C_T	surface transfer coefficient for heat
C_1	soil transfer coefficient for moisture
C_2	soil transfer coefficient for moisture
C_3	soil transfer coefficient for moisture
d_1	superficial soil depth
d_2	total soil depth
d_{soil}	soil column depth
d_{veg}	vegetation root depth
E	total evaporation rate
E_g	bare soil evaporation rate
E_{tr}	transpiration rate
E_r	evaporation rate from the interception reservoir (interception loss)
H	sensible heat flux
H_u	surface relative humidity
K_w	hydraulic conductivity
K_{sat}	hydraulic conductivity at saturation
L	latent heat of vaporization
LAI	leaf area index
P	precipitation rate
P_v	precipitation rate above the canopy
P_g	flux of liquid water reaching the soil surface
q_a	specific humidity at the first level of the atmospheric model
$q_{sat}(T)$	specific humidity at saturation at temperature T
R_a	aerodynamic resistance
R_r	drainage rate form the interception reservoir
R_s	canopy surface resistance
R_{smin}	minimum stomatal resistance
R_n	net radiation
T_s	surface temperature
T_2	mean surface temperature
T_c	climatological deep soil temperature
veg	fraction of vegetation cover
veg_{max}	maximum fraction of vegetation cover
w_{fc}	volumetric water content at field capacity
w_g	surface volumetric water content
w_{geq}	surface volumetric water content when gravity balances the capillarity forces
w_{sat}	volumetric water content at saturation
w_{wilt}	volumetric water content at wilting point
w_2	mean volumetric water content
W_r	water content of the interception reservoir
W_{rmax}	maximum water content of the interception reservoir
Z_0	roughness length for momentum transfers
Z_{0H}	roughness length for heat and water vapor transfers
Z_{0v}	contribution of vegetation to the roughness length
Z_{0rel}	contribution of subgrid-scale orography to the roughness length
α	surface albedo
α_{veg}	vegetation albedo
α_{soil}	bare soil albedo
δ	percentage of liquid water on leaves
Δt	time step of the model
ϵ	surface emissivity
γ	maximum amount of liquid water a foliage can retain
μ	fraction of grid box covered by rainfall
φ	generic variable
ψ	dimensionless soil moisture

density of air
density of liquid water
restore constant of 1 day
restore constant of 20 days

APPENDIX B

Estimation of the C_3 Coefficient

ie C_3 coefficient characterizes the velocity at which vater profile is restored to the field capacity. As- ng that the only sink of water over a soil column produced by gravitational drainage at the bottom e layer, the prognostic equation for w_2 takes the

$$\frac{\partial w_2}{\partial t} = -\frac{K_w}{d_2}. \tag{B1}$$

equation can be integrated starting from saturation using the following relation between the hydraulic uctivity K_w and the volumetric water content w_2:

$$K_w = K_{\text{sat}}\left(\frac{w_2}{w_{\text{sat}}}\right)^{2b+3}. \tag{B2}$$

water content at time t is given by

$$_2(t) = w_{\text{sat}}\left[1 + (2b+2)\frac{K_{\text{sat}}}{d_2 w_{\text{sat}}}t\right]^{-1/(2b+2)}. \tag{B3}$$

: evolution of w_2 is given by a Newtonian restore

$$\frac{\partial w_2}{\partial t} = -C_3\frac{w_2 - w_{fc}}{\tau_1}, \tag{B4}$$

olumetric water content w_2^* for $t = \tau_1/C_3$ starting saturation is

$$w_2^* = w_{fc} + (w_{\text{sat}} - w_{fc})/e. \tag{B5}$$

acing this value in Eq. (B3) provides an estimate e coefficient C_3:

$$C_3 = \frac{\tau_1(2b+2)K_{\text{sat}}}{d_2 w_{\text{sat}}[(w_2^*/w_{\text{sat}})^{-2b-2} - 1]}. \tag{B6}$$

textural dependency of this coefficient can be fitted power law with the fraction of clay X_{clay}:

$$C_3 = \frac{5.32X_{\text{clay}}^{-1.042}}{d_2}. \tag{B7}$$

time constant increases for finer soil textures. For l depth of 1 m, a sand is restored in 14 h toward capacity and a clay in 10 days.

REFERENCES

, J. C., J. P. Goutorbe, and A. Perrier, 1986: HAPEX-MOBILHY: A hydrologic atmospheric experiment for the study of water budget and evaporation flux at the climatic scale. *Bull. Amer. Meteor. Soc.*, **67**, 138–144.

Arino, O., G. Dedieu, and P. Y. Deschamps, 1991: Accuracy of satellite land surface reflectance determination. *J. Appl. Meteor.*, **30**, 960–972.

Beljaars, A. C. M., and P. Viterbo, 1994: Sensitivity of winter evaporation to the formulation of aerodynamic resistance in the ECMWF model. *Bound.-Layer Meteor.*, **71**, 135–149.

Benkiran, C., and N. Cerisier, 1993: Etude de l'impact climatique de la déforestation Amazonienne. Note de travail ENM, Météo-France. [Available from CNRM, 42 Ave. Coriolis, 31057 Toulouse Cedex, France.]

Betts, A. K., and Harshvardan, 1987: Thermodynamic constraint on the cloud liquid water feedback in climate models. *J. Geophys. Res.*, **92**, 8483–8485.

Bougeault, P., 1985: A simple parameterization of the large-scale effect of cumulus convection. *Mon. Wea. Rev.*, **113**, 2108–2121.

——, B. Bret, P. Lacarrère, and J. Noilhan, 1991a: An experiment with an advanced surface parameterization in a meso-beta-model. Part II: The 16 June 1986 simulation. *Mon. Wea. Rev.*, **119**, 2374–2392.

——, J. Noilhan, P. Lacarrère, and P. Mascart, 1991b: An experiment with an advanced surface parameterization in a meso-beta-model. Part I: Implementation. *Mon. Wea. Rev.*, **119**, 2358–2373.

Braud, I., J. Noilhan, P. Bessemoulin, P. Mascart, R. Haverkamp, and M. Vauclin, 1993: Bare-ground surface heat and water exchanges under dry conditions: Observations and parameterization. *Bound.-Layer Meteor.*, **66**, 173–200.

Cess, R. D., and G. L. Potter, 1987: Exploratory studies of cloud radiative forcing with a general circulation model. *Tellus*, **39A**, 460–473.

Charney, J. G., W. J. Quirks, S. H. Chow, and J. Kornfield, 1977: A comparative study of the effects of albedo change on drought in semi-arid regions. *J. Atmos. Sci.*, **34**, 1366–1385.

Clapp, R. B., and G. M. Hornberger, 1978: Empirical equations for some hydraulic properties. *Water Resour. Res.*, **14**, 601–604.

Deardorff, J. W., 1977: A parameterization of the ground surface moisture content for use in atmospheric predictions models. *J. Appl. Meteor.*, **16**, 1182–1185.

——, 1978: Efficient prediction of ground temperature and moisture with inclusion of a layer of vegetation. *J. Geophys. Res.*, **83**, 1889–1903.

Déqué, M., E. Cordoneanu, and J.-F. Geleyn, 1992: Initialisation des constantes climatologiques du modèle ARPEGE. Note de travail ARPEGE 21, Météo-France. [Available from CNRM, 42 Ave. Coriolis, 31057 Toulouse Cedex, France.]

——, C. Dreveton, A. Braun, and D. Cariolle, 1994: The ARPEGE/IFS atmosphere model: A contribution to the French community climate modelling. *Climate Dyn.*, **10**, 249–266.

Dickinson, R. E., 1984: Modeling evapotranspiration for three-dimensional global climate models. *Climate Processes and Climate Sensitivity, Geophys. Monogr.*, No. 29, American Geophysical Union, 58–72.

——, 1988: The force-restore method for surface temperatures and its generalization. *J. Climate*, **1**, 1086–1097.

——, 1989: Implications of the tropical deforestation for climate: A comparison of model and observational descriptions of surface energy and hydrological balance. *Philos. Trans. Roy. Soc. London B*, **324**, 423–431.

Dolman, A. J., and D. Gregory, 1992: A parameterization of rainfall interception in GCMs. *Quart. J. Roy. Meteor. Soc.*, **118**, 455–467.

Dorman, J. L., and P. J. Sellers, 1989: A global climatology for albedo, roughness length and stomatal resistance for atmospheric general circulation models as represented by the Simple Biosphere model (SiB). *J. Appl. Meteor.*, **28**, 833–855.

Ducoudré, N. I., K. Laval, and A. Perrier, 1993: SECHIBA, a new set of parameterizations of the hydrological exchanges of the land–atmosphere interface with the LMD atmospheric general circulation model. *J. Climate*, **6**, 248–273.

Dümenil, L., and E. Todini, 1992: A rainfall-runoff scheme for use in the Hamburg climate model. *Adv. Theor. Hydrol.*, **9**, 129–157.

Eagleson, P. S., N. M. Fennessey, Q. Wang, and I. Rodrigez-Iturbe, 1987: Application of spatial Poisson models to air mass thunderstorm rainfall. *J. Geophys. Res.*, **92**(D8), 9661–9678.

Eltahir, E. A. B., and R. L. Bras, 1993: Estimation of the fractional coverage of rainfall in climate models. *J. Climate*, **6**, 639–644.

Garratt, J. R., and B. B. Hicks, 1973: Momentum, heat and water vapour transfers to and from natural and artificial surfaces. *Quart. J. Roy. Meteor. Soc.*, **99**, 680–687.

——, P. K. Krummel, and E. A. Kowalczyk, 1993: The surface energy balance at local and regional scales—a comparison of general circulation model results with observations. *J. Climate*, **6**, 1090–1109.

Germain, M. J., 1990: Validation d'une paramétrisation des échanges de surface sur differents types de végétation. Note de travail ENM, Météo-France. [Available from CNRM, 42 Ave. Coriolis, 31057 Toulouse Cedex, France.]

Giordani, H., 1991: Représentation des échanges de surface dans les modèles météorologiques. Note de travail ENM, Météo-France. [Available from CNRM, 42 Ave. Coriolis, 31057 Toulouse Cedex, France.]

Goutorbe, J. P., J. Noilhan, C. Valancogne, and R. H. Cuenca, 1989: Soil moisture variations during HAPEX-MOBILHY. *Ann. Geophys.*, **7**, 415–426.

——, T. Lebel, A. Tinga, P. Bessemoulin, J. Brouwer, A. J. Dolman, E. T. Engman, J. H. C. Gash, M. Hopffner, P. Kabat, Y. H. Kerr, B. Monteny, S. Prince, F. Said, P. Sellers, and J. S. Wallace, 1994: HAPEX-Sahel: A large-scale study of land–atmosphere interactions in semi-arid Tropics. *Ann. Geophys.*, **12**, 53–64.

Henderson-Sellers, A., Z.-L. Yiang, and R. E. Dickinson, 1993: The project for intercomparison of land-surface parameterization schemes. *Bull. Amer. Meteor. Soc.*, **74**, 1335–1349.

Henning, D., 1989: *Atlas of the Surface Heat Balance of the Continents*. Gebrueder Borntraeger, 402 pp.

Hortal, M., and A. J. Simmons, 1991: Use of reduced Gaussian grids in spectral models. *Mon. Wea. Rev.*, **119**, 1057–1074.

Jacobsen, I., and E. Heise, 1982: A new economic method for the computation of the surface temperature in numerical models. *Contrib. Atmos. Phys.*, **55**, 128–141.

Jacquemin, B., and J. Noilhan, 1990: Sensitivity study and validation of a land surface parameterization using the HAPEX-MOBILHY data set. *Bound.-Layer Meteor.*, **52**, 93–134.

Köppen, W., 1923: *Die Klimate der Erde*. Walter de Gruyter, 369 pp.

Koster, R. D., and M. J. Suarez, 1992: Modeling the land surface boundary in climate models as a composite of independent vegetation stands. *J. Geophys. Res.*, **97**, 2697–2715.

Legates, D. R., and C. J. Willmott, 1990a: Mean seasonal and spatial variability in gauge-corrected, global precipitation. *Int. J. Climate*, **10**, 117–127.

——, and ——, 1990b: Mean seasonal and spatial variability in global surface air temperature. *Theor. Appl. Climatol.*, **41**, 11–21.

Louis, J. F., 1979: A parametric model of vertical eddy fluxes in the atmosphere. *Bound.-Layer Meteor.*, **17**, 187–202.

——, M. Tiedke, and J.-F. Geleyn, 1981: A short history of the PBL parameterization at the ECMWF. *Workshop on Planetary Boundary Layer Parameterization*, Shinfield Park, Reading, United Kingdom, ECMWF, 59–80.

Mahdaoui, F. El, 1994: Sensibilité du modèle ARPEGE-CLIMAT à la prise en compte de champs d'origine satellitaire. Note de travail ENM 457, Météo-France. [Available from CNRM, 42 Ave. Coriolis, 31057 Toulouse Cedex, France.]

Mahfouf, J. F., 1990: A numerical simulation of the surface moisture budget during HAPEX-MOBILHY. *Bound.-Layer Meteor.*, **53**, 201–222.

——, and B. Jacquemin, 1989: A study of rainfall interception using a land surface parameterization for mesoscale meteorological models. *J. Appl. Meteor.*, **28**, 1282–1302.

——, and J. Noilhan, 1991: Comparative study of various formulations of evaporation from bare soil using in-situ data. *J. Appl. Meteor.*, **30**, 1354–1365.

——, and ——, 1993: Le programme d'intercomparison de schémas de surface PILPS: Description des résultats obtenus avec ISBA. Note de centre GMME 17, Météo-France. [Available from CNRM, 42 Ave. Coriolis, 31057 Toulouse Cedex, France.]

Manzi, A. O., 1993: Introduction d'un schéma des transferts végétation-atmosphère dans un modèle de circulation générale et application à la déforestation amazonienne. Ph.D. thesis, Université Paul Sabatier, Toulouse, France, 229 pp.

——, and S. Planton, 1994: Implementation of the ISBA parameterization scheme for land surface processes in a GCM: An annual cycle experiment. *J. Hydrol.*, **155**, 355–389.

Mascart, P., J. Noilhan, and H. Giordani, 1995: A modified parameterization of the surface layer flux-profile relationships using different roughness length values for heat and momentum. *Bound.-Layer Meteor.*, in press.

Matthews, E., 1985: Atlas of archived vegetation, land-use and seasonal albedo. Tech. Rep. 86199, NASA, GISS, New York, 53 pp.

Milliman, J. D., and R. H. Meade, 1983: World-wide delivery of river sediment to the oceans. *J. Geol.*, **91**, 1–21.

Mintz, Y., and Y. V. Serafini, 1992: A global monthly climatology of soil moisture and water balance. *Climate Dyn.*, **8**, 13–27.

Noilhan, J., and S. Planton, 1989: A simple parameterization of land surface processes for meteorological models. *Mon. Wea. Rev.*, **117**, 536–549.

——, and P. Lacarrère, 1995: GCM gridscale evaporation from mesoscale modeling. *J. Climate*, **8**, 206–223.

——, ——, and Ph. Bougeault, 1991: An experiment with an advanced surface parameterization in a meso-beta-model. Part II: Comparison with the HAPEX-MOBILHY data set. *Mon. Wea. Rev.*, **119**, 2393–2413.

——, J. F. Mahfouf, A. Manzi, and S. Planton, 1993: Validation of land-surface parameterizations: Developments and experiments at the French Weather Service. *Validation of the Models over Europe*, ECMWF, 125–158.

Pitman, A. J., and A. Henderson-Sellers, 1993: Sub-grid scale precipitation in AGCMs: Re-assessing the land surface sensitivity using a single column model. *Climate Dyn.*, **9**, 33–41.

——, Z. L. Yang, J. C. Cogley, and A. Henderson-Sellers, 1991: Description of bare essentials of surface transfer for the Bureau of Meteorology Research Centre AGCM. Tech. Rep. 32, BMRC, Melbourne, Australia, 86 pp.

Ritter, B., and J.-F. Geleyn, 1992: A comprehensive radiation scheme for numerical weather prediction models with potential applications in climate simulations. *Mon. Wea. Rev.*, **120**, 303–325.

Russell, G. L., and J. R. Miller, 1990: Global river runoff calculated from a global atmospheric general circulation model. *J. Hydrol.*, **117**, 241–254.

Rutter, A. J., K. A. Kershaw, P. C. Robins, and A. J. Morton, 1971: A predictive model of rainfall interception in forests. Part I: Derivation of the model from observations in a plantation of Corsican pine. *Agric. Meteor.*, **9**, 367–384.

Sellers, P. J., Y. Mintz, Y. C. Sud, and A. Dalcher, 1986: A Simple Biosphere model (SiB) for use within general circulation models. *J. Atmos. Sci.*, **43**, 505–531.

——, W. J. Shuttleworth, J. L. Dorman, A. Dalcher, and J. M. Roberts, 1989: Calibrating the Simple Biosphere model for Amazonian tropical forest using field and remote sensing data. Part I: Average calibration with field data. *J. Appl. Meteor.*, **28**, 727–759.

Serafini, Y. V., 1990: The time scale of land surface hydrology in response to initial soil moisture anomalies: A case study. *Tellus*, **42A**, 390–400.

Shukla, J., and Y. Mintz, 1982: Influence of land-surface evapotranspiration on the earth's climate. *Science*, **215**, 1498–1501.

Shuttleworth, W. J., 1988a: Macrohydrology: The new challenge for process hydrology. *J. Hydrol.*, **100**, 31–56.

1988b: Evaporation from Amazonian rainforest. *Proc. Roy. Soc. London B*, **233**, 321–346.
1989: Micrometeorology of temperate and tropical forest. *Phil. Trans. Roy. Soc. London B*, **324**, 299–334.
and R. E. Dickinson, 1989: Comments on "Modelling tropical deforestation: A study of GCM land-surface parameterizations" by R. E. Dickinson and A. Henderson-Sellers. *Quart. J. Roy. Meteor. Soc.*, **115**, 1177–1179.
J. H. C. Gash, C. R. Lloyd, J. Roberts, A. de O. Marques, J. Fisch, V. de P. Silva, M. N. G. Ribiero, L. C. B. Molion, L. D. A. de Sa, J. C. Nobre, O. M. R. Cabral, S. R. Patel, and J. C. Moraes, 1984: Eddy correlation of energy partition for Amazonian forest. *Quart. J. Roy. Meteor. Soc.*, **110**, 1143–1162.
rt, J. B., 1988: Modelling surface conductance of pine forest. *Agric. For. Meteor.*, **43**, 19–35.
——, and S. B. Verma, 1992: Comparison of surface fluxes and conductances at two contrasting sites within the FIFE area. *J. Geophys. Res.*, **97**, 18 623–18 628.
Sud, Y. C., J. Shukla, and Y. Mintz, 1988: Influence of land surface roughness on atmospheric circulation and precipitation: A sensitivity study with a general circulation model. *J. Appl. Meteor.*, **27**, 1036–1054.
Webb, R. S., C. E. Rosenzweig, and E. R. Levine, 1991: A global dataset of soil particle size properties. Tech. Rep. 4286, NASA, GISS, New York, 34 pp.
Wetzel, P. J., and J. T. Chang, 1987: Concerning the relationship between evapotranspiration and soil moisture. *J. Climate Appl. Meteor.*, **26**, 18–27.
Wilson, M. F., and A. Henderson-Sellers, 1985: A global archive of land cover and soils data sets for use in general circulation climate models. *J. Climatol.*, **5**, 119–143.